

Repulsion of a Néel-Type Skyrmion from a Pearl Vortex in Thin Ferromagnet–Superconductor Heterostructures

E. S. Andriyakhina^{a, b}, S. Apostoloff^a, and I. S. Burmistrov^{a, c, *}

^a Landau Institute for Theoretical Physics, Russian Academy of Sciences,
Chernogolovka, Moscow region, 142432 Russia

^b Moscow Institute for Physics and Technology (National Research University), Moscow, 141700 Russia

^c Laboratory for Condensed Matter Physics, National Research University Higher School of Economics,
Moscow, 101000 Russia

*e-mail: burmi@itp.ac.ru

Received October 16, 2022; revised October 22, 2022; accepted October 25, 2022

In this paper we study repulsion of a Néel-type skyrmion in a chiral ferromagnetic film from a superconducting Pearl vortex due to the stray fields. Taking into account an effect of the vortex magnetic field on the skyrmion non-perturbatively, we find that the repulsion between them is suppressed with increase in the dimensionless strength of the vortex magnetic field. This manifests itself in complicated evolution of the free energy with increase in the vortex magnetic field and reduction of the equilibrium distance between the centers of Néel-type skyrmion and Pearl vortex.

DOI: 10.1134/S0021364022602512

INTRODUCTION

Mutual influence of magnetism and superconductivity in heterostructures has long history of research [1–5]. Recently, superconductor–ferromagnet (SF) bilayers hosting topologically nontrivial magnetic configurations have attracted much attention [6–8]. Such topologically stable configurations can be stabilized by Dzyaloshinskii–Moriya interaction (DMI) in ferromagnetic films [9]. Skyrmions in SF heterostructures induce Yu–Shiba–Rusinov-type bound states [10, 11], host Majorana modes [12–20], affect the Josephson effect [21], and change the superconducting critical temperature [22].

Skyrmions and superconducting vortices can form bound pairs in SF heterostructures due to interplay of spin–orbit coupling and proximity effect [23, 24]. In addition, vortices and skyrmions interact via stray fields [25–28]. Recently, stable skyrmion-vortex coexistence has been experimentally observed in $[\text{Ir}_1\text{Fe}_{0.5}\text{Co}_{0.5}\text{Pt}_1]^{10}/\text{MgO}/\text{Nb}$ sandwich structure [29].

In [28] two of the authors predicted that a Néel-type skyrmion and a Pearl vortex interacting via stray fields are repelled from each other to be located at a finite distance. However, the analysis of [28] has been limited to the lowest order perturbation theory in the magnetic field induced by the vortex.

In this work, we study interaction between a superconducting Pearl vortex and a Néel-type skyrmion in

a chiral ferromagnetic film due to stray fields (see Fig. 1). Contrary to [28], we take into account the change of the skyrmion profile due to magnetic field induced by the Pearl vortex. Performing non-perturbative treatment of the effect of vortex magnetic field on the one hand by analytical approach and on the other hand by micromagnetic modeling, we find that the free energy \mathcal{F} of the system as a function of the distance a between the skyrmion and the vortex experiences drastic changes with increase in the dimensionless strength γ of the vortex magnetic field, cf. Eq. (6). In particular, \mathcal{F} has (i) the single minimum at $a = a_{\min} > 0$ for $\gamma < \gamma_{\text{cr},-}$, (ii) two minima at $a = 0$ and at $a = a_{\min}$ with $\mathcal{F}(0) > \mathcal{F}(a_{\min})$ for $\gamma_{\text{cr},-} < \gamma < \gamma_{\text{cr}}$, (iii) two minima at $a = 0$ and at $a = a_{\min}$ with $\mathcal{F}(0) < \mathcal{F}(a_{\min})$ for $\gamma_{\text{cr}} < \gamma < \gamma_{\text{cr},+}$, and (iv) the single minimum at $a = 0$ for $\gamma_{\text{cr},+} < \gamma$ (cf. Fig. 2). With increase in γ the distance a_{\min} between the centers of a Néel-type skyrmion and a Pearl vortex is reduced and jumps to zero abruptly at $\gamma = \gamma_{\text{cr},+}$ (cf. Fig. 3). All three critical values $\gamma_{\text{cr},\pm}$ and γ_{cr} depend on the dimensionless DMI strength (cf. Fig. 4). In general, we can make somewhat counter-intuitive statement: the repulsion between the skyrmion and the vortex is suppressed with increase in the dimensionless vortex magnetic field.

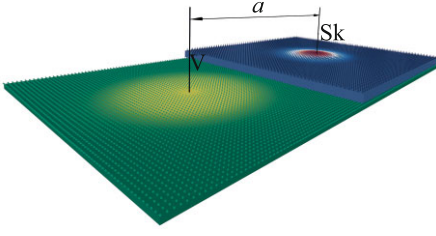


Fig. 1. (Color online) Sketch of a ferromagnet (blue)–superconductor (green) heterostructure. A thin insulating layer is not shown. The ferromagnetic layer hosts a Néel-type skyrmion (Sk). The superconducting film hosts a vortex (V). The distance between their centers is a .

SKYRMION–VORTEX INTERACTION

Following [28], our setup consists of ferromagnetic and superconducting films of thicknesses d_F and d_S , respectively. We assume that both films are thin, $d_S \ll \lambda_L$ and $d_F \ll R$, where λ_L is the London penetration length and R denotes the skyrmion radius. In addition, we assume the presence of a thin insulating layer between superconducting and ferromagnetic films in order to suppress the proximity effect. The superconducting film hosts a pair of Pearl vortex and antivortex separated by a distance much larger than the Pearl penetration length $\lambda = \lambda_L^2/d_S$ [30] (see Fig. 1).

The free energy of a thin chiral ferromagnetic film subjected to the magnetic field \mathbf{B}_V produced by a Pearl vortex is given by

$$\mathcal{F}[\mathbf{m}] = d_F \int d^2\mathbf{r} \{ A(\nabla\mathbf{m})^2 + D[m_z \nabla \cdot \mathbf{m} - (\mathbf{m} \cdot \nabla)m_z] + K(1 - m_z^2) - M_s \mathbf{m} \cdot \mathbf{B}_V|_{z=+0} \}. \quad (1)$$

Here, $\mathbf{m}(r)$ is the unit vector along direction of the magnetization \mathbf{M} , M_s stands for saturation magnetization of the film. The exchange, DMI, and perpendicular anisotropy energy constants are denoted as A , D , and K , respectively. We assume that these parameters are positive, $A, K, D > 0$. The magnetic field of the Pearl vortex centered at the position with coordinate a is given as [31]:

$$\mathbf{B}_V = \phi_0 \text{sgn}(z) \nabla \int \frac{d^2\mathbf{q}}{(2\pi)^2} \frac{e^{-q|z|+iq(\mathbf{r}-\mathbf{a})}}{q(1+2q\lambda)}, \quad (2)$$

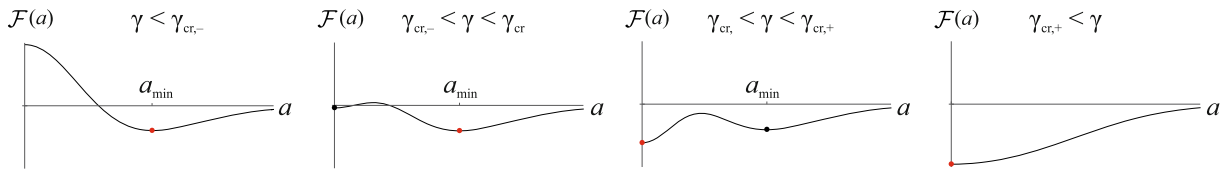


Fig. 2. (Color online) Sketch of dependence $\mathcal{F}(a)$ for different ranges of γ . Left panel, $\gamma < \gamma_{cr,-}$: There is the single minimum at nonzero distance a_{\min} . Middle panel with $\gamma_{cr,-} < \gamma < \gamma_{cr}$: There is the global minimum at nonzero distance a_{\min} and the local one at $a = 0$. Middle panel with $\gamma_{cr} < \gamma < \gamma_{cr,+}$: There is the global minimum at zero distance $a = 0$ and the local one at a_{\min} . Right panel, $\gamma_{cr,+} < \gamma$: There is the single minimum at $a = 0$.

where $\phi_0 = hc/2e$ denotes the flux quantum. The free energy $\mathcal{F}[\mathbf{m}]$ is normalized in such a way that $\mathcal{F} = 0$ for the ferromagnetic state, $m_z = 1$, and without the Pearl vortex, $\mathbf{B}_V = 0$. We note that we neglect interaction between the skyrmion and antivortex situated at a large distance away.

SHIFTED SKYRMION AT $\gamma \rightarrow 0$

In the absence of the vortex the magnetization corresponding to a Néel-type skyrmion can be sought in the cylindrical coordinate system as [32]

$$\mathbf{m} = \mathbf{e}_r \sin \theta(r) + \mathbf{e}_z \cos \theta(r). \quad (3)$$

Minimizing the free energy $\mathcal{F}[\mathbf{m}]$ with $\mathbf{B}_V = 0$ with respect to a skyrmion angle $\theta(r)$, one can derive the Euler–Lagrange equation,

$$\ell_w^2 \Delta_r \theta(r) - \frac{(\ell_w^2 + r^2)}{2r^2} \sin 2\theta(r) + 2\epsilon \frac{\sin^2 \theta(r)}{r/\ell_w} = 0. \quad (4)$$

Here a dimensionless parameter $\epsilon = D/2\sqrt{AK}$ controls the strength of DMI, the domain wall width $\ell_w = \sqrt{A/K}$ sets a natural length scale in the problem and $\Delta_r \theta = \partial_r(r\partial_r\theta)/r$ is the radial part of Laplacian.

In order to solve Eq. (4) one needs to specify the boundary conditions. Assuming naturally that the film is ferromagnetically magnetized away from the skyrmion, $\theta(r \rightarrow \infty) = 0$ ($m_z = 1$). At the center of the skyrmion magnetization has the opposite direction, $m_z = -1$. Since at $\epsilon > 0$ only skyrmions of positive chirality are stabilized in the ferromagnet, $m_z = -1$ corresponds to the condition $\theta(r \rightarrow 0) = \pi$.

Knowing the solution $\theta(r) = \theta_0(r)$ of Eq. (4) (in the absence of the vortex magnetic field), we can calculate [28] the interaction energy as a function of distance a between the centers of the skyrmion and the vortex,

$$\frac{\delta\mathcal{F}(a)}{4\pi A d_F} = \gamma \int_0^\infty dr r \{ b_r^a(r) \sin \theta_0(r) + b_z^a(r) [\cos \theta_0(r) - 1] \}, \quad (5)$$

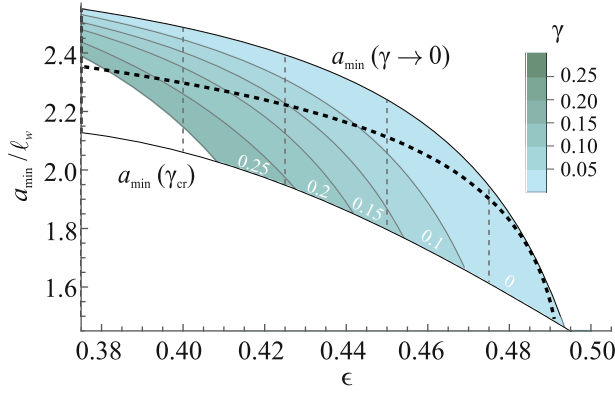


Fig. 3. (Color online) Distance a_{\min} between the skyrmion and the vortex versus ϵ for several values of γ ranging from 0.01 to 0.3. The dashed curve illustrates analytical prediction for $a_{\min}(\epsilon)$ $\gamma \rightarrow 0$, see text below Eq. (8). For each value of ϵ the distance a_{\min} varies from $a_{\min}(\gamma \rightarrow 0)$ to $a_{\min}(\gamma_{\text{cr}})$. Once γ becomes larger than γ_{cr} , the system reaches coaxial phase. The shaded regions guide the constant value of the vortex strength γ , see the color bar inset.

where the dimensionless strength γ of the vortex magnetic field is given as

$$\gamma = (\ell_w / \lambda)(M_s \phi_0 / 8\pi A). \quad (6)$$

Equation (5) is valid in the leading approximation on small vortex strength $\gamma \ll 1$. Notation $\delta\mathcal{F}$ means that we subtract the energy of the lonely skyrmion itself and the energy of the homogeneous ferromagnet in the vortex field from the total free energy $\mathcal{F}[\mathbf{m}]$. The functions $b_r^a(r)$ and $b_z^a(r)$ means the dimensionless r - and z -projections of the vortex field \mathbf{B}_V averaged by rotation of the system around the center of the skyrmion, i.e., over all possible directions of the vector a . They are given as

$$b_{r/z}^a(r) = 2\ell_w \int_0^\infty \frac{dq q J_0(qa) J_{1/0}(qr)}{(\lambda^{-1} + 2q)}. \quad (7)$$

Assuming the skyrmion radius to be much smaller than the Pearl length, $R \ll \lambda$, that requires $d_S \ll \lambda_L^2 / R$, we can treat the functions $b_{r/z}^a(r)$ in the limit $r \sim R \ll \lambda$ as

$$b_z^a(r) \approx \frac{2\ell_w}{\pi(a+r)} K\left(\frac{4ar}{(a+r)^2}\right), \quad (8)$$

$$b_r^a(r) \approx (\ell_w / r) \Theta(r - a).$$

Here, $\Theta(z)$ denotes the Heaviside step function and $K(z)$ is the complete elliptic integral of the first kind.

The minimum of $\delta\mathcal{F}(a)$ determines the stable position a_{\min} of the skyrmion. The resulting dependence of a_{\min} on ϵ at $\gamma \rightarrow 0$ is shown in Fig. 3 by the dashed line. As one can see, a_{\min} is of the order of $2\ell_w$ and decreases with increase in ϵ .

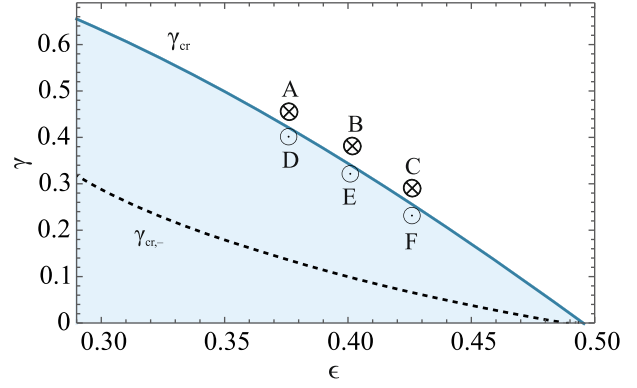


Fig. 4. (Color online) Phase diagram. The solid curve shows dependence $\gamma_{\text{cr}}(\epsilon)$ extracted from micromagnetic simulations. The black dashed curve corresponds to $\gamma_{\text{cr},-}(\epsilon)$. In the blue shaded region, the distance between the skyrmion and the vortex is nonzero, $a_{\min} > 0$, cf. Fig. 2. The points A–F correspond to the respective panels (a–f) in Fig. 5.

It should be emphasized that in the analysis above we neglect a change of the skyrmion profile due to the vortex field when calculating Eq. (5). Indeed, such a reshaping should be taken into account in the next approximation on small vortex strength γ . For small γ an account of the next order correction leads only to a small correction of the magnitude of a_{\min} , but does not change the result qualitatively.

NEARLY CENTERED SKYRMION, $a \rightarrow 0$

Now we study at what parameters the coaxial configuration of the skyrmion and the vortex ($a = 0$) is unstable. The magnetization of such skyrmion also can be sought as given by Eq. (3), due to the radial symmetry of the problem. Then the minimization of the free energy $\mathcal{F}[\mathbf{m}]$ with respect to the skyrmion angle $\theta(r)$ yields the Euler–Lagrange equation similar to Eq. (4), but with $\gamma[b_r^0(r) \cos \theta(r) - b_z^0(r) \sin \theta(r)]$ instead of zero in the right hand side. Boundary conditions remain the same: $\theta(r \rightarrow \infty) = 0$ and $\theta(r \rightarrow \infty) = \pi$.

When the solution $\theta(r) = \theta_\gamma(r)$ for a finite magnitude of γ is obtained, we can calculate the interaction energy $\delta\mathcal{F}(a)$ for small $a \ll \ell_w$. The idea is the same as beyond Eq. (5). For small spacing a , one can neglect the reshaping of the skyrmion in the leading approximation and use Eq. (5), but with $\theta_\gamma(r)$,

$$\frac{\delta\mathcal{F}(a) - \delta\mathcal{F}(0)}{4\pi A d_F} = \gamma \int_0^\infty dr r \{ \delta b_r^a(r) \sin \theta_\gamma(r) + \delta b_z^a(r) [\cos \theta_\gamma(r) - 1] \}. \quad (9)$$

Here we introduce $\delta b_{r/z}^a(r) = b_{r/z}^a(r) - b_{r/z}^0(r)$. At $r \sim R \ll \lambda$ and $a \rightarrow 0$ these functions can be estimated as $\delta b_z^a(r) \approx \ell_w a^2 / (4r^3)$ and $\delta b_r^a(r) \approx \ell_w a^2 / (8r^2 \lambda)$. Note that though the result (9) has been obtained in the limit of small a , it allows to predict the existence of a minimum of $\mathcal{F}(a)$ at $a = 0$ for an arbitrary value $\gamma > 0$.

At $\gamma \rightarrow 0$ and for $\epsilon < \epsilon_{\text{cr},-} \approx 0.488$ the free energy has a maximum at $a = 0$, because $\delta \mathcal{F}(a) < \delta \mathcal{F}(0)$. Hence, the skyrmion is repelled from the vortex in agreement with [28]. With increase in γ the difference $\delta \mathcal{F}(a) - \delta \mathcal{F}(0)$ changes sign at $\gamma = \gamma_{\text{cr},-}$ and the minimum at $a = 0$ appears in the free energy. Therefore, for $\gamma > \gamma_{\text{cr},-}$ the skyrmion can be stable right at the vortex. The dependence of $\gamma_{\text{cr},-}$ on ϵ extracted from Eq. (9) is shown in Fig. 4 by the dashed curve. As one can see $\gamma_{\text{cr},-}$ decreases with increase in ϵ and vanishes at $\epsilon_{\text{cr},-} \approx 0.488$. We expect similar dependence of $\gamma_{\text{cr},+}$ on ϵ . Our theoretical analysis demonstrates that $\gamma_{\text{cr},+}$ vanishes at $\epsilon_{\text{cr},+} \approx 0.493$ which is only slightly larger than $\epsilon_{\text{cr},-}$. We note that γ_{cr} vanishes at the value of $\epsilon_{\text{cr}} \approx 0.491$ which lies between $\epsilon_{\text{cr},-}$ and $\epsilon_{\text{cr},+}$. We stress that with relevant precision $\epsilon_{\text{cr},-} \simeq \epsilon_{\text{cr}} \simeq \epsilon_{\text{cr},+} \approx 0.49$.

MICROMAGNETIC MODELING

To explore the skyrmion stable state in the field of the Pearl vortex with change of ϵ and γ , we perform micromagnetic simulations. We utilize Object Oriented MicroMagnetic Framework (OOMMF) [33] by dint of Ubermag [34] Python packages.

The system is modeled as a set of classical magnetic vectors placed in the center of mesh cells. The distance is measured in units of the domain wall width ℓ_w . We note that for the micromagnetic modeling we set the magnetic anisotropy parameter $K = 1$ and DMI $D = 2\epsilon$. Periodical boundary conditions (in xy -plane) are imposed to simulate an isolated region of a ferromagnet–insulator–superconductor structure. We create a skyrmion by initiating a closed region with a flipped magnetization and letting it relax in the presence of the Heisenberg exchange, DMI and magnetic anisotropy interactions as well as in the vortex-induced magnetic field.

We point out that the system is not subject to any other external fields, so that the only source of Zeeman energy comes from the interaction with the vortex. In our simulations we consider a Pearl vortex with zero-sized core to be pinned in the origin of the grid, see Eq. (2).

The micromagnetic simulations allow us to find the dependence of the distance a_{min} between the skyrmion and the vortex on ϵ for a finite value of γ , see Fig. 3. As

in the case of $\gamma \rightarrow 0$, a_{min} decreases with increase in ϵ at constant magnitude of γ . Similarly, a_{min} decreases with the increase in γ at a constant value of ϵ . We note a discrepancy between the theory and the micromagnetic simulations that becomes more prominent for smaller ϵ , see Fig. 3. We believe that this happens due to discretization effects which are inevitable in the numerical approach. In our simulations we have found that by making the mesh finer, one observes the declining tendency for a_{min} towards the theoretical value marked by the dashed curve in Fig. 3. However, for small values of ϵ one needs to account both for smaller mesh cells and for larger sample size, which is computationally expensive.

The results of micromagnetic simulations are consistent with evolution of the free energy with γ illustrated in Fig. 2 schematically. The phase diagram in ϵ and γ plane extracted from the obtained results is shown in Fig. 4. Two phases of stable position of the skyrmion, right on the top of the vortex (white clear upper region) and at the finite distance a_{min} (blue shaded lower region), are separated by the solid line $\gamma = \gamma_{\text{cr}}(\epsilon)$. One can see that γ_{cr} drops to zero when ϵ reaches approximately 0.49 in accordance with theoretical predictions. As we have mentioned above there is the lower and upper critical values $\gamma_{\text{cr},\mp}(\epsilon)$ at which minimum at $a = a_{\text{min}} > 0$ disappears and minimum at $a = 0$ appears, respectively. However, we cannot resolve these values within our micromagnetic modeling.

The skyrmion profiles obtained by means of micromagnetic simulations for ϵ and γ corresponding to the points A, B, and C in Fig. 4 are presented in Fig. 5 (upper row). As expected, in all three cases skyrmions are situated right on the top of the vortex, i.e., $a_{\text{min}} = 0$. In lower row of Fig. 5 we demonstrate skyrmions for parameters ϵ and γ corresponding to the points D, E, and F in Fig. 4. In this case the nonzero distance of the skyrmion from the vortex is clearly seen.

We draw a reader's attention to the spatial structure of the magnetization of the shifted skyrmions corresponding to the points D, E, and F. Naturally, as the effective strength γ of the vortex magnetic field increases, the magnetization profile deviates from the radially symmetric one. This leads to the following. Firstly, the center of the skyrmion is getting closer the center of the vortex, and secondly, the radius of the skyrmion increases. In addition to that, the projection of the magnetization on the xy plane (shown as black arrows in Fig. 5) partially aligns along the direction of the magnetic field. These changes in the profile lead to a decrease in the total free energy $\mathcal{F}(a_{\text{min}})$ of the displaced skyrmion as a function of γ . However, the free energy $\mathcal{F}(a = 0)$ of a skyrmion placed exactly above the vortex decreases faster with increasing γ . As a consequence, when γ exceeds γ_{cr} , the energy of the shifted

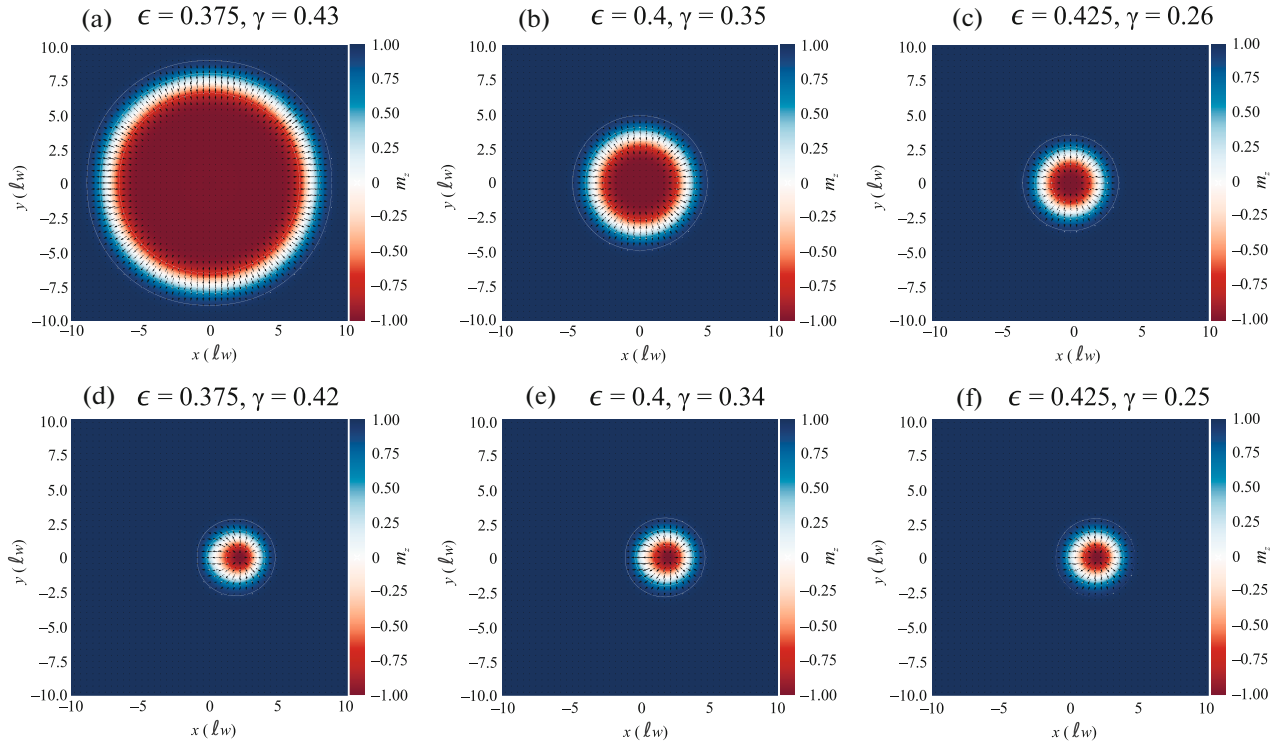


Fig. 5. (Color online) Distributions of magnetization for different values of ϵ and γ . The Pearl vortex is located at the center of each picture, i.e., at $x = y = 0$. The white contours illustrate a level set of the m_z projection. The most extreme contour in each panel separates the skyrmion magnetization from purely ferromagnetic spin ordering. The black arrows reflect the magnitude and direction of the projection of the magnetization \mathbf{m} on the xy plane. The upper row corresponds to vortex strength γ slightly above the critical γ_{cr} , when skyrmion abruptly changes its position and becomes coaxial with the vortex. The lower row illustrates distribution of m_z for γ which is slightly less than γ_{cr} , i.e., for the case of nonzero a_{min} . One can clearly see that the skyrmions in the lower row are shifted from the sample's center where the Pearl vortex is settled. The panels (a–f) match with the respective points A–F marked in Fig. 4.

skyrmion becomes greater than the energy of the skyrmion located exactly above the vortex.

To clarify significance of critical values of dimensionless vortex strength $\gamma_{cr,\pm}$ and γ_{cr} let us consider the case of small but finite concentration of skyrmions and vortices. Then at $\gamma < \gamma_{cr,-}$ one can expect the phase of (dipole-like) pairs consisting of skyrmion and vortex separated by a distance a_{min} . At $\gamma > \gamma_{cr,+}$ one can observe the phase of (point-like) pairs of skyrmion and vortex sitting on the top of each other. In the intermediate range $\gamma_{cr,-} < \gamma < \gamma_{cr,+}$ there is the phase in which there are finite concentrations of dipole-like and point-like skyrmion-vortex pairs. Under assumption that the system can reach the global minimum of the free energy, there will be a true thermodynamic transition at γ_{cr} between the phases with dipole-like and point-like pairs, respectively. Since the dimensionless vortex strength γ depends on material parameters, see Eq. (6), and is proportional to the thickness of superconducting film d_S , it could be possible to see the transitions described above with thickness change.

SUMMARY

In this work, we have extended the study of interaction between a superconducting Pearl vortex and a Néel-type skyrmion in a chiral ferromagnetic film to non-perturbative regime with respect to the stray fields induced by the vortex. Contrary to the previous work [28] of two of us limited to the regime of a weak dimensionless vortex magnetic field, $\gamma \rightarrow 0$, we have found that the increase in γ suppresses repulsion of skyrmion and vortex and leads to reduction of the distance a_{min} between the centers of a Néel-type skyrmion and a Pearl vortex as shown in Fig. 3. Most surprisingly, we have discovered the existence of interesting evolution of the free energy of the system with γ . In particular, at $\gamma < \gamma_{cr,-}$ the free energy $\mathcal{F}(a)$ has the only minimum at $a = a_{min}$ whereas at $\gamma > \gamma_{cr,+}$ it has the only minimum at $a = 0$, see Figs. 2 and 4.

Finally, we mention that it would be interesting to generalize our results to the case of skyrmions and vortices in confined geometries, e.g., nanodots etc. [35–37], skyrmion-vortex lattices [38], as well as to more exotic magnetic excitations, e.g., antiskyrmions, bimerons, biskyrmions, skyrmioniums, etc. [7].

ACKNOWLEDGMENTS

We are grateful to A. Fraerman, M. Kuznetsov, and M. Shustin for useful discussions and to O. Tretiakov and P. Vorobyev for collaboration on a related project. We acknowledge the computing time provided to us at computer facilities at Landau Institute.

FUNDING

The work was supported by the Russian Science Foundation, project no. 21-42-04410.

CONFLICT OF INTEREST

The authors declare that they have no conflicts of interest.

OPEN ACCESS

This article is licensed under a Creative Commons Attribution 4.0 International License, which permits use, sharing, adaptation, distribution and reproduction in any medium or format, as long as you give appropriate credit to the original author(s) and the source, provide a link to the Creative Commons license, and indicate if changes were made. The images or other third party material in this article are included in the article's Creative Commons license, unless indicated otherwise in a credit line to the material. If material is not included in the article's Creative Commons license and your intended use is not permitted by statutory regulation or exceeds the permitted use, you will need to obtain permission directly from the copyright holder. To view a copy of this license, visit <http://creativecommons.org/licenses/by/4.0/>.

REFERENCES

1. V. V. Ryazanov, V. A. Oboznov, A. S. Prokofiev, V. V. Bolginov, and A. K. Feofanov, *J. Low Temp. Phys.* **136**, 385 (2004).
2. I. F. Lyuksyutov and V. L. Pokrovsky, *Adv. Phys.* **54**, 67 (2005).
3. A. I. Buzdin, *Rev. Mod. Phys.* **77**, 935 (2005).
4. F. S. Bergeret, A. F. Volkov, and K. B. Efetov, *Rev. Mod. Phys.* **77**, 1321 (2005).
5. M. Eschrig, *Rep. Prog. Phys.* **78**, 104501 (2015).
6. C. Back, V. Cros, H. Ebert, K. Everschor-Sitte, A. Fert, M. Garst, T. Ma, S. Mankovsky, T. L. Monchesky, M. Mostovoy, N. Nagaosa, S. S. P. Parkin, C. Pfeiderer, N. Reyren, A. Rosch, Y. Taguchi, Y. Tokura, K. von Bergmann, and J. Zang, *J. Phys. D: Appl. Phys.* **53**, 363001 (2020).
7. B. Göbel, I. Mertig, and O. A. Tretiakov, *Phys. Rep.* **895**, 1 (2021).
8. A. O. Zlotnikov, M. S. Shustin, and A. D. Fedoseev, *J. Supercond. Nov. Magn.* **34**, 3053 (2021).
9. A. N. Bogdanov and D. Yablonskii, *Sov. Phys. JETP* **68**, 101 (1989).
10. S. S. Pershoguba, S. Nakosai, and A. V. Balatsky, *Phys. Rev. B* **94**, 064513 (2016).
11. K. Pöyhönen, T. Ojanen, A. Westström, S. S. Pershoguba, and A. V. Balatsky, *Phys. Rev. B* **94**, 214509 (2016).
12. W. Chen and A. P. Schnyder, *Phys. Rev. B* **92**, 214502 (2015).
13. G. Yang, P. Stano, J. Klinovaja, and D. Loss, *Phys. Rev. B* **93**, 224505 (2016).
14. U. Güngördü, S. Sandhoefner, and A. A. Kovalev, *Phys. Rev. B* **97**, 115136 (2018).
15. E. Mascot, S. Cocklin, S. Rachel, and D. K. Morr, *Phys. Rev. B* **100**, 184510 (2019).
16. S. Rex, I. V. Gornyi, and A. D. Mirlin, *Phys. Rev. B* **100**, 064504 (2019).
17. M. Garnier, A. Mesaros, and P. Simon, *Commun. Phys.* **2**, 126 (2019).
18. S. Rex, I. V. Gornyi, and A. D. Mirlin, *Phys. Rev. B* **102**, 224501 (2020).
19. U. Güngördü and A. A. Kovalev, *J. Appl. Phys.* **132**, 041101 (2022).
20. J. Nothhelfer, S. A. Díaz, S. Kessler, T. Meng, M. Rizzi, K. M. D. Hals, and K. Everschor-Sitte, *Phys. Rev. B* **105**, 224509 (2022).
21. T. Yokoyama and J. Linder, *Phys. Rev. B* **92**, 060503(R) (2015).
22. V. A. Tumanov, V. E. Zaitseva, and Yu. N. Proshin, *JETP Lett.* **116**, 449 (2022).
23. K. M. D. Hals, M. Schecter, and M. S. Rudner, *Phys. Rev. Lett.* **117**, 017001 (2016).
24. J. Baumard, J. Cayssol, F. S. Bergeret, and A. Buzdin, *Phys. Rev. B* **99**, 014511 (2019).
25. S. M. Dahir, A. F. Volkov, and I. M. Eremin, *Phys. Rev. Lett.* **122**, 097001 (2019).
26. R. M. Menezes, J. F. S. Neto, C. C. de Souza Silva, and M. V. Milošević, *Phys. Rev. B* **100**, 014431 (2019).
27. S. M. Dahir, A. F. Volkov, and I. M. Eremin, *Phys. Rev. B* **102**, 014503 (2020).
28. E. S. Andriyakhina and I. S. Burmistrov, *Phys. Rev. B* **103**, 174519 (2021).
29. A. P. Petrović, M. Raju, X. Y. Tee, A. Louat, I. Maggio-Aprile, R. M. Menezes, M. J. Wyszyński, N. K. Duong, M. Reznikov, Ch. Renner, M. V. Milosević, and C. Panagopoulos, *Phys. Rev. Lett.* **126**, 117205 (2021).
30. J. Pearl, *Appl. Phys. Lett.* **5**, 65 (1964).
31. A. A. Abrikosov, *Fundamentals of the Theory of Metals* (North-Holland, Amsterdam, 1988).
32. Y. Kawaguchi, Y. Tanaka, and N. Nagaosa, *Phys. Rev. B* **93**, 064416 (2016).
33. M. J. Donahue and D. G. Porter, OOMMF User's Guide, Version 1.0, Interagency Report NISTI No. 6376 (1999).
34. M. Beg, M. Lang, and H. Fangohr, *IEEE Trans. Magn.* **58**, 1 (2022).
35. S. Rohart and A. Thiaville, *Phys. Rev. B* **88**, 184422 (2013).
36. V. L. Vadimov, M. V. Sapozhnikov, and A. S. Mel'nikov, *Appl. Phys. Lett.* **113**, 032402 (2018).
37. L. González-Gómez, J. Castell-Queralt, N. Del-Valle, and C. Navau, *Phys. Rev. Appl.* **17**, 034069 (2022).
38. J. F. Neto and C. C. de Souza Silva, *Phys. Rev. Lett.* **128**, 057001 (2022).